Pure Appl. Geophys. 168 (2011), 2221–2237

DOI 10.1007/s00024-011-0273-7

Pure and Applied Geophysics

A Unifying Phase Diagram for the Dynamics of Sheared Solids and Granular Materials

Yehuda Ben-Zion,[1] Karin A. Dahmen,[2] and Jonathan T. Uhl[3]

Abstract—We present a simple unifying model that can be used to analyze, within a single framework, different dynamic regimes of shear deformation of brittle, plastic, and granular materials. The basic dynamic regimes seen in the response of both solids and granular materials to slowly increasing loading are scale-invariant behavior with power law statistics, quasi-periodicity of system size events, and persisting long term mode switching between the former two types of response. The model provides universal analytical mean field results on the statistics of failure events in the different regimes and distributed versus localized spatial responses. The results are summarized in a phase diagram spanned by three tuning parameters: dynamic strength change (weakening, neutral or strengthening) during slip events, dissipation of stress transfer (related to the void fraction in granular materials and damaged solids), and the ratio of shear rate over healing rate controlling the regaining of cohesion following failures in brittle solids. The mean field scaling predictions agree with experimental, numerical, and observational data on deformation avalanches of solids, granular materials, and earthquake faults. The model provides additional predictions that should be tested with future observation and simulation data.

Key words: irreversible deformation, damaged rocks, solid mechanics, granular mechanics, phase transitions, brittle deformation, plastic deformation.

1. Introduction

In the last 20 years considerable progress has been made in studies of disordered materials and their jerky avalanche-like response to a slowly changing driving force (e.g., Turcotte, 1997; Sethna *et al*., 2001; Zaiser, 2006; Avala *et al*., 2006; Dahmen and Ben-Zion, 2009). Example applications include deformation of crystals and lab-size materials, crackling noise in magnetic systems, and seismicity in the crust of the Earth. Traditional approaches can be divided broadly into continuum and discrete models, and the choice of using one versus the other is typically made based on the scale and topic of interest (e.g., Ben-Zion, 2008). However, recent lab experiments of nominally smooth plastic deformation reveal step-like stress–strain curves (with power law-distributed step sizes) and the formation of localized slip-bands on the sample surface (e.g., Zaiser, 2006). This closely resembles the long length scale behavior of the deformation of brittle solids and sheared granular materials in the solid phase (e.g., Lyakhovsky *et al*., 2001; Liu and Nagel, 2001; Aharonov and Sparks, 2004).

The brittle upper crust contains, in general, a mixture of damaged rocks and granular materials, with various distributions of cracks and particles that change rapidly in close spatio-temporal proximity to the occurrence of brittle instabilities. Motivated by diverse multi-scale lab and field observations, and various theoretical results from different frameworks, Ben-Zion (2008) suggested that crustal materials near active faults undergo repeating two-way phase transitions between solid and granular states of rocks (or mathematically continuum-discrete transitions). Multiple episodes of brittle deformation associated with earthquakes lead to material evolution from a competent solid through damaged rock to granular material, while material healing in the interseismic periods produces evolution in the opposite direction (Ben-Zion, 2008, Section 7).

Many models have been developed to study the response of materials under shear loading, with applications on scales ranging from sub-microns (dislocation dynamics) to hundreds of kilometers (earthquake fault dynamics). Dislocation-based (e.g., Weertman, 1996; Zaiser, 2006; Csikor *et. al.*, 2007)

[1] Department of Earth Sciences, University of Southern California, Los Angeles, CA 90089-0740, USA. E-mail: benzion@usc.edu

[2] Department of Physics, University of Illinois at Urbana Champaign, 1110 West Green Street, Urbana, IL 61801, USA.

[3] Los Angeles, USA.

and Shear Transformation Zone or STZ (e.g., Spaepen, 1977; Bulatov and Argon, 1994; Falk and Langer, 1998) models are based on atomistic frameworks and can describe plastic deformation, but they do not account for internal surfaces (cracks), evolving elastic moduli and other features of brittle deformation. Damage rheology models address the evolution of elastic moduli and related aspects of deformation (e.g., Kachanov, 1986; Ashby and Sammis, 1990; Lyakhovsky and Ben-Zion, 2008), but they do not account for granular mechanics. Models of granular mechanics (e.g., Jaeger *et al*., 1996; Aharonov and Sparks, 1999; Liu and Nagel, 2001; Rechenmacher *et al*., 2010) can explain transitions in the behavior of granular material under different conditions, but they do not account for plastic, damage, and other aspects of solid deformation. Developing a bridge between solid and granular modes of deformation and material phases can provide a powerful unifying framework for many theoretical and observational results concerned with large irreversible deformation.

In the present paper we propose a simple unifying framework for analysis of brittle, plastic, and granular deformations, and the transitions between continuum and discrete phases of materials. The analysis builds on analytical results obtained with mean field theory (MFT) for three variants of the Ben-Zion and Rice (BZR) model, developed originally to study earthquake dynamics (Ben-Zion and Rice, 1993; Fisher *et al*., 1997; Dahmen *et al*., 1998) and extended recently to study dislocation slips in sheared crystals (Dahmen *et al*., 2009) and slip avalanches in sheared granular media (Dahmen *et al*., 2011). The striking similarities in observations associated with slip avalanches in different systems (e.g., Turcotte, 1997; Zaiser, 2006) are reflected by similarities in the assumptions and predictions of the three variants of the BZR model. Even though these model variants describe different physical systems, their analytical mean field analyses are closely related. Based on the connections between the various model versions, predicted analytical results, observations, and numerical simulations, we propose a unified picture of avalanche dynamics in these different systems.

Our analyses of slip avalanches in solid and granular materials share the following assumptions. (1) The measured slip avalanche statistics reflect the steady state dynamics of the system. This is a common assumption used in most experiments, observations and models. (2) The slip avalanches are statistically uniformly distributed, either in the bulk or along a fault plane. This assumption is made in many other models as well. (3) The boundaries are loaded slowly either by increasing shear stress or motion with a small fixed velocity. This is true in various experiments and is also true for earthquake systems driven by slow tectonic loading. (4) As the system is slowly sheared, weak spots fail, and stress is transferred through long range elastic interactions, leading to failure avalanches. This is seen in the experiments and observations that we are modeling. (5) The interactions are sufficiently long range ($1/\text{distance}^3$) so that MFT yields the correct scaling behavior on long scales in the physical dimension. In MFT the physical interactions are replaced by infinite range interactions, and the equations can usually be solved analytically, yielding exact analytic scaling predictions on long length scales. This assumption is supported by renormalization group calculations and by numerical simulations which show that the scaling behaviors are the same in MFT and in systems with full 3D elastic stress transfer functions (Fisher *et al*., 1997; Dahmen *et al*., 1998, 2009; Ben-Zion *et al*., 2003; Mehta *et al*., 2006).

The model is reviewed briefly in the next section with an emphasis on three basic ingredients that serve as tuning parameters of the dynamics: (1) a strength-change parameter ε during failure (or slip) episodes, (2) effective porosity $(1 - cv)$ with v being a grain volume fraction controlling the conservation of elastic stress transfer during failure episodes, and (3) a ratio Q between the shear rate and healing rate of brittle solids that governs the amount of cohesion along surfaces (cracks) in contact. Building on key previous and new analytical results we construct a phase diagram for different dynamic regimes of deformation in solid and granular media. The phase diagram is accompanied by comparisons (Table 1) between analytical scaling exponents predicted by the model for statistics of slip avalanches in different systems, available observational results, and simulations. The results indicate overall agreement (within error bars) between MFT predictions, experiments and

Table 1

Comparisons between analytical model predictions based on mean field theory, laboratory experiments, earthquake observations, and simulations for various systems

Exponent or other universal quantity	**Mean Field Theory**	**Granular experiments [1-8]**	**Granular simulations [9-10]**	**Dislocation experiments [11-14]**	**Earthquake data [15,16]**	**Damage rheology [17-19]**
τ (size distribution)	1.5	1.5	?	1.5-1.8	1.4-2.2	1.3-2.5
$1/\sigma vz$ (power spectrum)	2 if $v \approx 1$; 0 if $v \ll 1$	1.8-2.5 2	2 if solid-like 0 if fluid-like	?	~2	?
α (duration distribution)	2	2	?	?	1.8 - 3.4	?
Source time function at fixed duration [12]	Symmetric (parabola) **[20]**	?	Symmetric: sine function (?)	?	asymmetric maybe?	?
CE/QP statistics	if $\varepsilon>0$ & $v>v^*$	some	mode switching	?	*Yes*	Yes
Mode switching between PL and CE	if $\varepsilon>0$ & $v>v^*$	?	In solid regime	?	*Yes*	Yes
Aftershocks (with Omori exponent p)	if $\varepsilon<0$ & slow healing, p=1	none (?)	None (?)	Yes, p=?	Yes, p=1	Yes, p=1

Question marks (?) denote experimental data needed to further test the predicted results. Additional MFT predictions not yet tested in experiments are $1/\sigma' = 1/\sigma'' = 2$, $v'z = v''z = 1$ (see text). The results in the shaded region are explained in more detail in Dahmen *et al*., 2011. PL, Power law; CE, Characteristic earthquake/event; QP, Quasi-periodicity. The numbers in the square brackets denote the following references: 1, Daniels *et al*. (2005); 2, Hayman *et al*. (2010); 3, Jaeger *et al*. (1996); 4, Zhang *et al*. (2010) ; 5, Yu *et al*. (2009) ; 6, Petri *et al*. (2008) ; 7, Baldassari *et al*. (2006); 8, Hartley (2004); 9, Aharonov and Spark (2002) ; 10, Aharonov and Spark (2004); 11, Richeton et al. (2005); 12, Dimiduk *et al*. (2006); 13, Miguel and Sapperi (2006); 14, Zaiser (2006); 15, Ben-Zion (2008); 16, Mehta *et al*. (2006); 17, Lyakhovsky (2001); 18, Ben-Zion *et al*. (1999); 19, Ben-Zion and Lyakhovsky (2006); 20, Kuntz and Sethna (2000)

simulations with granular materials, experiments and simulations in solids sustaining plastic deformation and brittle damage, and observations associated with seismicity in the Earth crust. Additional analytical model predictions should be tested with future observational and simulation results.

2. Model

The employed model provides a simple representation for systems with heterogeneities, evolving threshold dynamics and long range interaction. The model is simple enough to be amenable to analytical understanding, yet sufficiently realistic to produce a diverse set of deformation phenomena consistent with observations (Ben-Zion, 2008, Section 5.2, and references therein). Here we only review the basic equations, key parameters and key dynamic regimes of the model. More detailed descriptions can be found in the references listed below in the context of the various discussed topics.

We assume that permanent shear deformation in a 3D material (Fig. 1) is governed by

$$\eta \partial u(\mathbf{r},t)/\partial t = F + \sigma_{\rm int}(\mathbf{r},t) - f_R[u,\mathbf{r},\{u(\mathbf{r},t'<t)\}], \quad (1)$$

where η is an effective viscosity, $u(\mathbf{r}, t)$ is the cumulative slip in the shear direction at point $\mathbf{r}$, F is the remotely applied shear stress, and $f_R[u, \mathbf{r}, \{(u(\mathbf{r}, t' < t)\}]$ is a local pinning stress that can vary randomly from place to place. The term

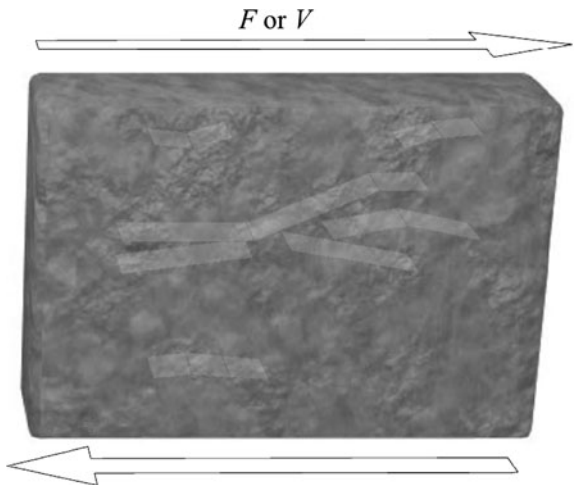

Figure 1
A solid with internal heterogeneities subjected to slowly increasing shear loading produced by either tangential stress F or tangential velocity V

$\sigma_{\rm int}(\mathbf{r}, t)$ accounts for stress produced by prior slips in the medium since time $t = 0$ and is given by

$$\sigma_{\rm int}(r,t) = \int_0^t dt' \int d^d r' J(r-r',t-t')[u(r',t') - u(r,t)], \tag{2}$$

where the exponent d denotes the dimension of the system and J is the stress transfer function. Equation 1 provides a general description of particle motion in a medium with distributed rather than concentrated mass (e.g., Fisher, 1998; Ben-Zion, 2008). In numerical simulations the employed J is based on the solution for dislocations in a 3D elastic half-space (Chinnery, 1963; Ben-Zion and Rice, 1993), while in derivations of the discussed analytical results a mean field version with a constant average stress transfer is used (Fisher *et al.*, 1997; Dahmen and Ben-Zion, 2009).

A discrete version of the model is obtained by considering a coarse grained three-dimensional cubic lattice of linear dimension L with $N = L^3$ sites. When the boundaries move with a small fixed velocity V, the MFT local stress τ_i at point i in the bulk and time t is given (e.g., Dahmen *et al.*, 1998; Mehta *et al.*, 2006) by

$$\tau_i = J/N \sum_m (u_m - u_i) + K_L(Vt - u_i), \tag{3}$$

where $u_{\rm m}$ is the total local slip at site m, J is the infinite range mean field elastic coupling strength, and K_L is the weak stiffness of the bulk that couples each site to the remote moving boundary, i.e., $F = K_L(Vt - u_i)$ with $K_L \sim J/L$ and small boundary velocity V. Increasing shear stress in the system can lead to sudden failure avalanche events followed by material re-healing. We consider two types of boundary conditions: a slowly increasing shear stress F or a small constant tangential velocity V (Fig. 1). The results presented in this paper (Sect. 3) are obtained using the discrete version of the model.

Each site i fails when the local stress reaches a failure threshold, which can be static or dynamic: $\tau_{f,i} \equiv \tau_{s,i}$ (or $\tau_{d,i}$). The failure threshold characterizes the amount of friction and/or cohesion C at a given position in the system and is quenched, but may vary in space due to material heterogeneities. The threshold for failing the first time in an avalanche is $\tau_{s,i}$. When a site i fails, it slips by amount Δu_i until its stress is reduced to an arrest level $\tau_{a,i}$ at which level it re-sticks. During failure the local threshold may change to a dynamic level $\tau_{d,i}$, which can be smaller or larger than the static level, augmented by some cohesion change ΔC in the case of brittle solids. The total strength change is given by $\Delta C + \varepsilon$, where $\varepsilon = (\tau_{s,i} - \tau_{d,i})/(\tau_{s,i} - \tau_{a,i})$, $\Delta C = (C_i^{\rm initial} - C_i^{\rm final})/(\tau_{s,i} - \tau_{a,i})$, and we assume that ΔC is zero for both granular materials and plastic deformation. At the end of each avalanche the dynamic friction levels reheal to their static values $\tau_{s,i}$, and in the case of brittle solids there is also a gradual cohesion regaining that depends on the ratio $Q =$ (shear-rate/healing-rate). The exact shapes of the distributions of $\tau_{s,i}$, $\tau_{d,i}$, $\tau_{a,i}$, and ΔC do not affect the universal scaling results reported below. In the following we set $\tau_{a,i} = 0$ and assume narrow parabolic distribution for $\tau_{s,i.}$ (e.g., Fisher *et al.*, 1997; Dahmen *et al.*, 2009). The values of $\tau_{d,i}$ are calculated from $\tau_{s,i}$ and ε. For cases representing brittle solids we assume that the reductions of ΔC during failures are also taken from a narrow distribution and are followed by gradual logarithmic-type recoveries. In the next section we provide a detailed algorithm for model calculations along with various results.

Numerous earlier studies with the BZR model version that corresponds to an earthquake fault have shown that ε acts as a tuning parameter of the dynamics (e.g., Fisher *et al.*, 1997; Dahmen and

Ben-Zion, 2009). Situations with $\varepsilon > 0$ represent dynamic weakening (Ben-Zion and Rice, 1993), cases with $\varepsilon < 0$ represent dynamic strengthening (Mehta *et al*., 2006), while the limit value $\varepsilon = 0$ corresponds to a critical depinning transition (Fisher *et al*., 1997). As illustrated in the next section, ε turns out to be a tuning parameter also in cases representing plastic deformation and avalanches in granular materials. The key role of ε may be understood intuitively by noticing that $\varepsilon > 0$ provides a positive feedback during deformation, while $\varepsilon < 0$ is associated with negative feedback. The former tends to produce for ranges of conditions (see next section) localization of deformation and quasi-periodic occurrence (i.e., coefficient of variations of recurrence intervals less than 1) of system-size events following the characteristic frequency-size distribution. In contrast, the latter tends to produce distributed deformation and frequency-size event statistics following a truncated power law (Dahmen *et al*., 2009, 2011). The limit neutral case $\varepsilon = 0$ is associated with a second-order phase transition and leads to scale invariant responses in space, time and energy/size domains (Fisher *et al*., 1997; Ben-Zion *et al*., 2003; Dahmen and Ben-Zion, 2009).

Another tuning parameter of the model is the degree of conservation of stress transfer during failure events quantified by a fractional dissipation parameter (Dahmen *et al*., 1998). A full conservation can exist only in infinite elastic solids, while in finite materials some fraction of the stress transfer (that would have been distributed to the domain beyond the material boundaries) is necessarily lost. In cases corresponding to deformation in solids, this also accounts for various forms of inelastic dissipation. In a model version that corresponds to granular material with a grain volume fraction v (Dahmen *et al*., 2011), the fractional dissipation is given by $(1 - cv)$. The degree of conservation of stress transfer, or the related dissipation parameter, is a second tuning parameter of the model dynamics. Previous studies demonstrated that for realistic ranges of parameters, with some dynamic weakening and some dissipation of stress transfer, the BZR model exhibits a mode switching response (Dahmen *et al*., 1998) involving spontaneous long-term fluctuations between two types of behavior: relatively quiet periods with power law distribution of small to intermediate size events, and highly active time intervals with clusters of large events following the characteristic distribution.

A different set of studies on similar topics, with a damage rheology model for coupled evolution of earthquakes and faults, have shown that the nondimensional number Q (= the ratio of time scales for material healing to loading, or shear-rate/healing-rate) also acts as a tuning parameter of the dynamics (e.g., Ben-Zion *et al*., 1999; Lyakhovsky *et al*., 2001). Situations with very large Q correspond to systems with long memory of weakening phases generated during brittle instabilities (consider, e.g., the limit case of no healing) and lead to localization of deformation and the characteristic frequency-size distribution. In contrast, situations with very small Q (consider, e.g., the limit case of instantaneous healing) have short memory and lead to sustained generation of disordered networks of faults and power law frequency-size event statistics. Intermediate values of Q produce a mode switching response in which the fault zone structures and seismicity patterns alternate, over long time intervals compared to large earthquake cycles, between the forgoing two modes of behavior. In our proposed phase diagram for the dynamics of failure events in solids with different rheologies and granular materials, Q plays the role of the third tuning parameter.

3. Results

As mentioned, we distinguish between loadings associated with imposed stress and velocity at the edge of the model (Fig. 1). The former tends to produce an accelerated failure process and localization, while the latter will lead for a range of conditions to a stable process and distributed deformation. This is easy to understand from basic considerations. Each failure event leads to increasing stress concentration at the ends of the slipping zone. Since constant stress boundary conditions inhibit internal stress relaxation, a failure process under such loading is likely to grow and become a system size event, unless a negative rheological feedback $\varepsilon < 0$ with sufficient amplitude exists. In contrast, the

growth of a failure zone under constant velocity boundary conditions (constant displacement for slow velocities and short times) is accompanied by internal stress relaxation, which tends to promote a stable process and migration of subsequent failures to other locations, unless there is positive feedback $\varepsilon > 0$ with large amplitude and long memory (slow healing). As summarized by Ben-Zion (2008, Section 6), constant stress boundary conditions provide appropriate loading for studies concerned with the development of through-going localizations and system-size events (i.e., analysis of processes preceding large mainshocks), whereas constant velocity or displacement boundary conditions provide appropriate loading for studies concerned with distributed relaxation processes following system-size events (i.e., aftershock sequences and other postseismic signals). Numerical simulations of long deformation histories with many cycles of system-size events should use mixed velocity-stress boundary conditions, such as variable boundary forces proportional to the slip-deficit between the far field plate motion and displacement at the boundary (Lyakhovsky and Ben-Zion, 2008).

In the following we first review results obtained recently with two versions of the model corresponding to plastic deformation in solids and avalanches in granular materials. Then we present simple generalizations that can provide a unified explanation for key dynamical regimes of shear deformation in solids and granular media under different conditions.

3.1. Plastic Deformation of Solids Under Shear

In a discrete version of MFT with N lattice points, the local stress at a lattice point is given by Eq. 3. When site i fails, it slips by a certain amount Δu_i resulting in a stress reduction $\tau_{f,i} - \tau_{a,i} \approx 2G\Delta u_i$ where $G \sim J$ is the effective elastic shear modulus and the local strain is proportional to $\sum_m u_m$. When the stress increases slowly to a critical yield level F_c, the solid responds with slip avalanches (strain steps) of size S (potency per volume). The following analytical results describe the micromechanics of plastic deformation in solids subjected to stress and velocity boundary conditions and having different ε values (Dahmen *et al.*, 2009).

3.1.1 Slowly Increasing Applied Shear Stress F

Zero weakening ($\varepsilon = 0$, $\tau_{s,i} = \tau_{d,i}$): when the stress approaches F_c, the system approaches a depinning transition which has been studied previously in other contexts (e.g., Fisher, 1998; Richeton *et al.*, 2005; Dimiduk *et al.*, 2006; Dahmen and Ben-Zion, 2009). The local slope of the stress–strain curve (the effective shear modulus G), is inversely proportional (Fig. 2a) to the mean avalanche size $\langle S \rangle$, i.e. it scales as $G \sim 1/\langle S \rangle \sim (F_c - F)^{(2-\tau)/\sigma} \sim (F_c - F)$ (Fisher *et al.*, 1997; Dahmen *et al.*, 2009). At the yield stress F_c, the distribution $D(S, F_c)$ of slip avalanche sizes follows a universal power law $D(S, F_c) \sim 1/S^{\tau}$ with a universal critical exponent $\tau = 1.5$ (Fig. 2b). Below but close to F_c, the distribution follows the same power law up to a maximum size $S_{\max} \sim (F_c - F)^{1/\sigma}$, with a universal exponent $\sigma = 0.5$. This is reflected by the large S scaling form $D(S, F) \sim 1/S^{\tau} D_{\text{cut}}(S(F_c - F)^{1/\sigma})$ with universal cutoff scaling function $D_{\text{cut}}(x) \sim A \exp(-Bx)$ and non-universal fitting constants A and B. Above yielding ($F > F_c$) all points keep slipping with a mean slip-rate that scales as $d\langle u \rangle/dt \sim (F - F_c)^{\beta}$ with a universal exponent $\beta = 1$ (Fisher *et al.*, 1997; Dahmen *et al.*, 2009). These analytical predictions agree with simulation results for dislocation dynamics (Zaiser, 2006; Miguel and Zapperi, 2006; Tsekenis and Dahmen, 2010).

At F_c the slip-rate power spectra $P(\omega, F_c)$ (i.e., the absolute square of the Fourier transform of the time dependent slip rate $\mathrm{d}\left(\sum_m u_m\right)/\mathrm{d}t$) is expected to scale with frequency ω as $P(\omega, F_c) \sim \omega^{-2}$ (Fig. 2c). For $F < F_c$ the power law levels off at frequencies below a cutoff $\omega_{\min} \sim (F_c - F)^{\nu z}$ with $\nu z = 1$. This is captured by the functional form $P(\omega, F) \sim \omega^{-2} fcn(\omega/(F_c - F))$ where $fcn(x)$ is a universal scaling function. The distribution of avalanche durations T is expected to scale as $D(T) \sim 1/T^{\alpha} D_{\text{scl}}(T(F_c - F)^{\nu z})$ with $\alpha = 2$, $\nu z = 1$ and $D_{\text{scl}}(x)$ a universal scaling function. For $\varepsilon = 0$ the slip in the system is, on average, distributed uniformly over the sample (ductile deformation). Simulations of slip distributions in related models (Chen *et al.*, 1991; Maloney *et al.*, 2009) indicate that, on average, the individual slip avalanches tend to be parallel to the shear direction. The shapes of the slip distributions of individual events are fractal and time histories of various

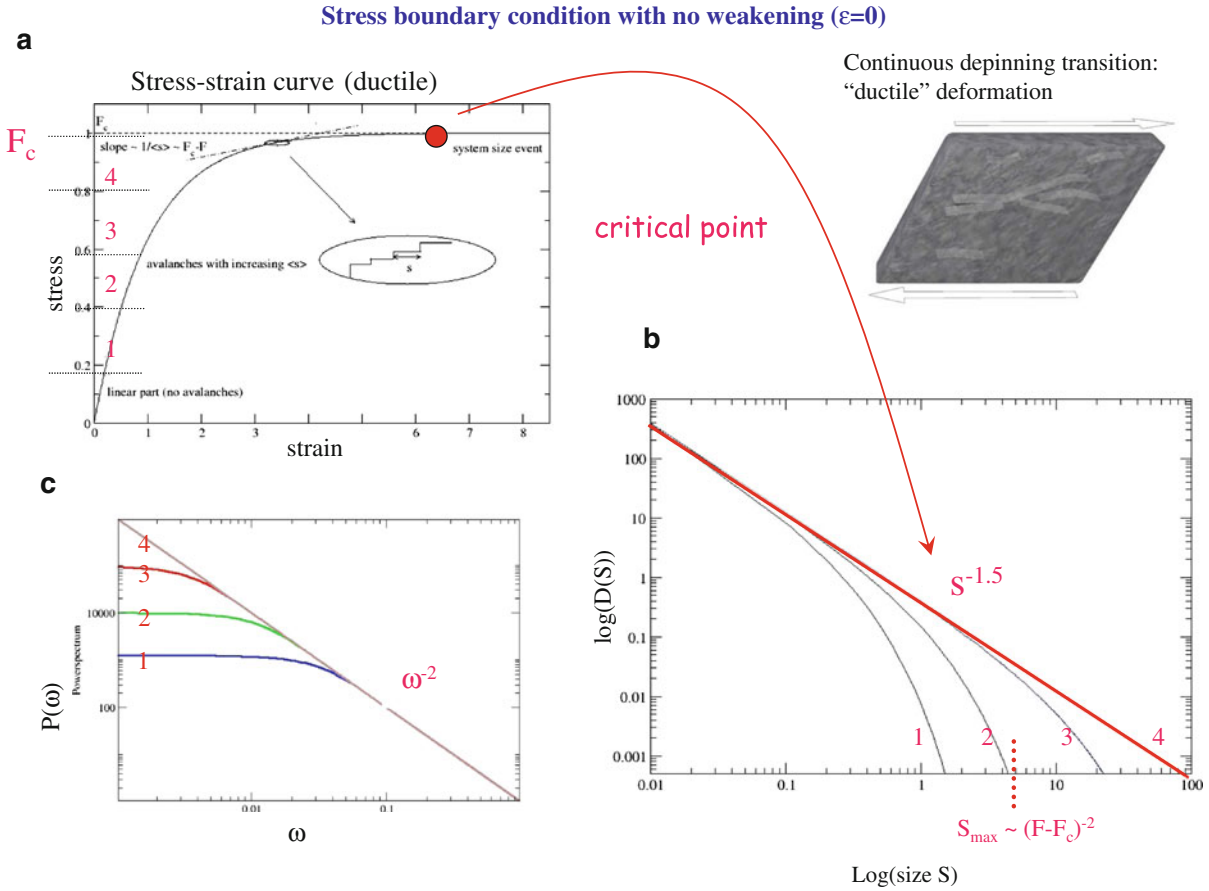

Figure 2

Analytical results on plastic deformation in solids with stress boundary condition and zero dynamic weakening ($\varepsilon = 0$). The dislocations are distributed in the volume and the overall mode of deformation is ductile. **a** Stress–strain curve as the shear stress is increased to the critical value F_c. The *red circle* denotes a critical (second order) depinning transition. **b** Frequency-size statistics of dislocation avalanches (*inset* in **a**) as the shear stress increases to F_c. **c** Power spectra of time histories of dislocation avalanches at different stress levels (Dahmen *et al.*, 2009)

quantities (e.g., average stress on fault and potency/magnitude vs. time) are scale invariant (Fisher *et al.*, 1997; Ben-Zion *et al.*, 2003).

Some weakening ($\varepsilon > 0$, $\tau_{s,i} > \tau_{d,i}$): here the deformation begins in a similar fashion but leads to brittle failure. Starting from a relaxed state, the material initially responds to an increasing shear stress $F < F_c(\varepsilon)$ with small avalanches, just like in the $\varepsilon = 0$ case. The yield stress $F_c(\varepsilon)$ is of order ε lower than the yield stress F_c for $\varepsilon = 0$ (Fisher *et al.*, 1997). The events are nucleated randomly throughout the system and thus lead in the initial stage, on average, to a uniform strain across the sample as with $\varepsilon = 0$. The frequency-size statistics follow a power law up to a stress dependent cutoff size $S_{\max} \sim \varepsilon^{-2} S((F_c - F)/\varepsilon)$. The power law distribution is $D(S) \sim 1/S^{\tau} D_w(S(F_c - F)^{1/\sigma}, S\varepsilon^2)$, with the same values $\tau = 1.5$ and $1/\sigma = 2$ as in the zero weakening case. At $F_c(\varepsilon) \equiv F_c - O(\varepsilon)$; however, the material breaks in brittle failure, i.e., the slip suddenly localizes in a system spanning avalanche that forms a narrow weakened failure or "fault zone" (Fig. 3). This is consistent with the expectation of Chen *et al.* (1991) based on a similar model. The shear modulus just before failure is $G \sim O(\varepsilon)$. In this case the system undergoes a discontinuous (first order) transition at $F_c(\varepsilon)$. We note that MFT may not capture correctly the detailed behavior in the brittle case just before localization when the dislocation density is very high in the localization region. Clarifying these

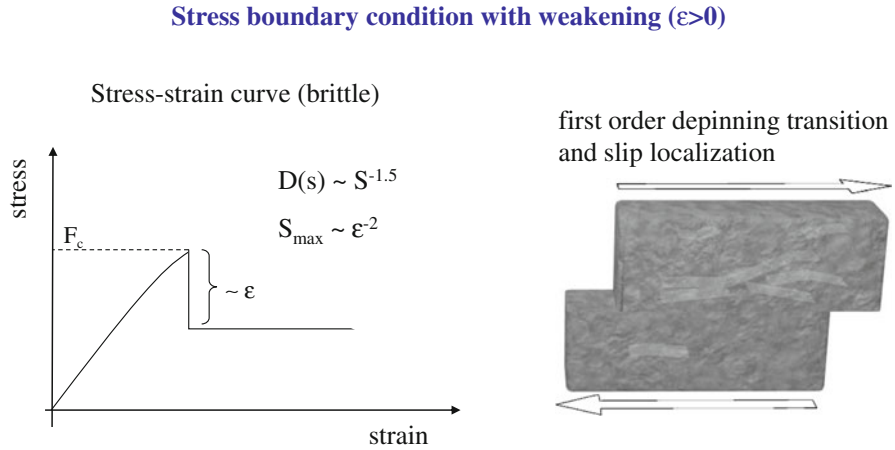

Figure 3
Analytical results on plastic deformation in solids with stress boundary condition and weakening ($\varepsilon > 0$). Here the deformation localizes and the overall mode of deformation is brittle (Dahmen *et al.*, 2009)

details will be the subject of future numerical work. After the system spanning fracture avalanche took place, continuous slip can be maintained (Fig. 3) at stresses that are $O(\varepsilon)$ less than the yield stress $F_c(\varepsilon)$.

Slip hardening ($\varepsilon < 0$, $\tau_{s,i} < \tau_{d,i}$): as in Mehta *et al.* (2006), hardening can be incorporated in the following way: if a site slips, the failure threshold of all other sites is either increased by an amount proportional to $|\varepsilon|/N$; or equivalently, the stresses at all cells are reduced by an amount $O(\varepsilon/N)$. Microscopically, this may correspond to the creation of dislocation pairs in the bulk that reduce the overall stress. This regime also corresponds to generation of dislocation entanglement, so that higher stress than in non-hardening systems is needed to trigger further events (Laurson and Alava, 2006). From the general discussion of hardening in Zaiser (2006) we conclude that $|\varepsilon|/N$ is proportional to the hardening coefficient θ of the material. In this case, for slowly increasing shear stress F from the relaxed state, the system first responds again with small avalanches like in the $\varepsilon = 0$ case. During a transient regime, their size distribution $D(S, F, \varepsilon)$ follows the power law $1/S^{\tau}$ (with $\tau = 1.5$) up to a cutoff size that increases with F. For larger stresses, hardening effects come into play and the system crosses over into a "steady state" regime with a power law distribution of avalanche sizes that is cut off at maximum size $S_{\max} \sim 1/\varepsilon^2$, i.e. $D(S, F, \varepsilon) \sim 1/S^{\tau} D_h(S\varepsilon^2)$ with universal exponent $\tau = 1.5$ as before. $D_h(x)$ is another universal scaling function. The slope of the stress–strain curve (Fig. 4a) scales as $G \sim 1/\langle S \rangle \sim |\varepsilon|$. In this regime the strain-rate power spectrum $P(\omega, F, \varepsilon)$ scales as $P(\omega, F, \varepsilon) \sim 1/\omega^2$ for high frequencies, with a low frequency cutoff $\omega_{\min} \sim \varepsilon$, i.e., the scaling form is given by $P(\omega, F, \varepsilon) \sim \omega^{-2} P_h(\omega/\varepsilon)$ where P_h is a universal scaling function. In the hardening regime, just as in the case for $\varepsilon = 0$, there is no slip localization, and the cumulative effect of all randomly nucleated avalanches is a distributed deformation of the solid. As illustrated in Fig. 4b, the discussed results are consistent with high-resolution observations of slip avalanches in hardening plastic regime (Dimiduk *et al.*, 2006).

3.2. Boundary Conditions of Tangential Velocity

With this type of boundary conditions, the mean field theory of the model becomes exactly as found earlier for a model version corresponding to a single pre-existing fault. The response for $\varepsilon = 0$ and full conservation of stress transfer consists of power law distribution of event sizes and all other results discussed above for the critical depinning transition, including scaling functions, exponent values, and fractal slip histories (Fisher *et al.*, 1997). With some weakening $\varepsilon > 0$, the slip distribution become

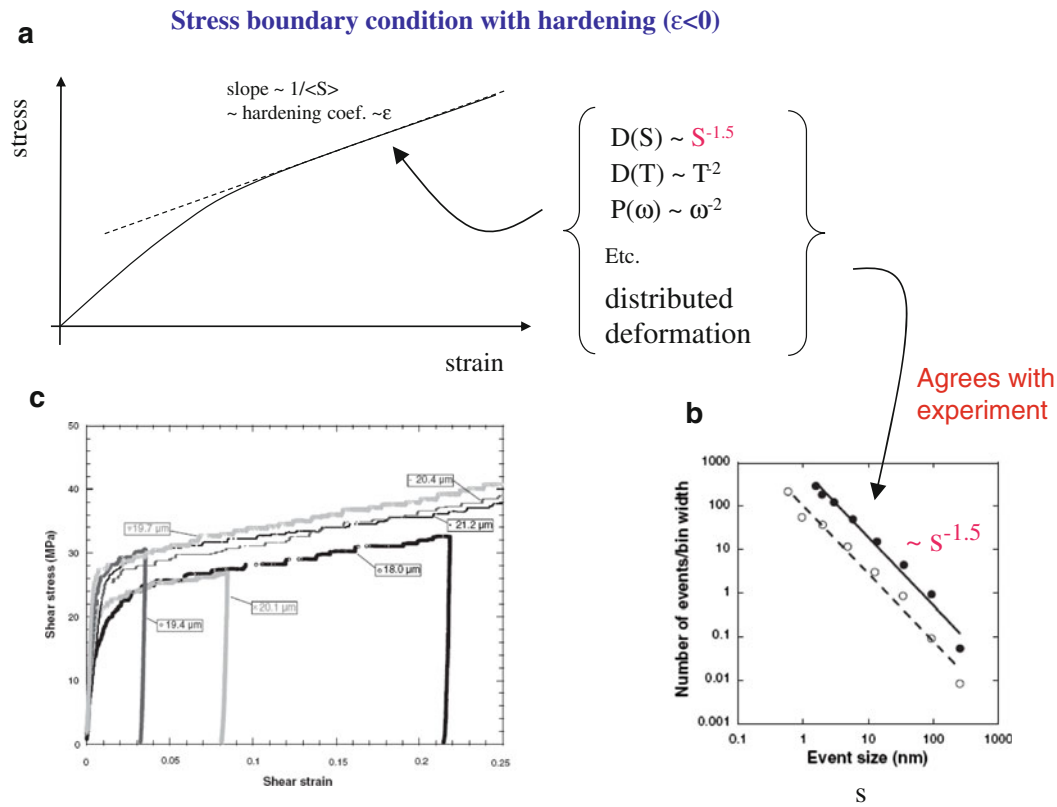

Figure 4

Analytical results on plastic deformation in solids with stress boundary condition and hardening ($\varepsilon < 0$). The dislocations are distributed in the volume and the overall mode of deformation is ductile. **a** Stress–strain curve for increasing shear stress and model predictions (for statistics of event sizes (S), duration (T), power spectra $P(\omega)$ of frequency (ω) corresponding to the regime indicated by the arrow). Etc. stands for additional scaling predictions for this regime derived in Dahmen *et al.* (2009). **b** Observed frequency-size statistics showing the number of slip events of a given size on a log–log plot in high resolution experiment of nominally plastic deformation (From Dimiduk *et al.*, 2006). Power law scaling over more than two orders of magnitude is exhibited for both a single sample approximately equal to 20 μm in diameter (*open circles* and *dashed line* fit) and the aggregate data from several samples (*solid circles* and *solid line* fit)(Dimiduk *et al.*, 2006). **c** Observed shear-stress versus shear-strain curves for Ni samples in high resolution experiments of nominally plastic deformation. The labels in boxes indicate sample diameters (From Dimiduk *et al.*, 2006)

compact, the events follow standard scaling relations for crack-like ruptures and the frequency-size statistics follow the characteristic earthquake distribution (Ben-Zion and Rice, 1993). For a range of parameters with some weakening and some dissipation of stress transfer, there is mode switching with spontaneous long-term fluctuations between time intervals with "undershoot" response and truncated power law statistics, and time intervals with "overshoot" response and the characteristic distribution (Dahmen *et al.*, 1998). For cases with hardening $\varepsilon < 0$, the response consists of slip events with power law frequency-size statistics and aftershocks (Mehta *et al.*, 2006). For conditions near the critical point ($\varepsilon = 0$ and no dissipation), the MFT potency/moment rate during a failure event (i.e., "source time function"), averaged over all events with the same duration, is a parabola of the form $Ax(1 - x)$. The average potency rate of events with the same final potency follows the exponential function $A_1 x \exp(-Bx^2/2)$. In these expressions, x stands for time rescaled by the total duration or moment, as appropriate, and A, A_1, B are non-universal constants (Mehta *et al.*, 2006).

3.3. Deformation of Sheared Granular Materials

The results discussed in the previous sections can also be used to understand, with some modifications

and appropriate mapping of variables, different dynamic regimes of shear granular media. At high grain volume fraction v, the grains are densely packed and the coarse grained system resembles a solid with randomly located voids, while at low v the system has fluid-like behavior. In Dahmen *et al.* (2011) it is shown how the MFT of a coarse grained lattice model that includes such voids can be mapped onto the MFT version of the BZR earthquake model analyzed earlier. The mapping indicates that the volume fraction v in the model for granular materials is directly proportional to the stress conservation parameter in the earthquake model. In other words the parameter $(1 - cv)$, with $c = J/(J + K_L)$ close to 1, plays the same role as the stress dissipation parameter of Dahmen *et al.* (1998). This stress dissipation parameter determines the fraction of a stress drop during a slip event that is redistributed to reload other regions in the granular medium.

The above mapping leads to the following results on the response of shear granular materials (Dahmen *et al.*, 2011). For $\varepsilon > 0$ and $v > v^*(\varepsilon)$, the MFT predicts the mode switching discussed in the previous section. The non-universal transition point $v^*(\varepsilon) = 1/(1 + \varepsilon)$ and the mean durations between consecutive mode switching events depend on details of the system (Dahmen *et al.*, 1998). The slip avalanche locations are randomly spread throughout the bulk of the granular medium, as seen in granular simulations (Aharonov and Sparks, 2002, 2004) and experiments (Hartley, 2004). For loosely packed grains ($v < v^*(\varepsilon)$), the mode switching disappears and the model predicts small avalanches, decreasing in size with decreasing volume fraction v. This regime is similar to the "fluid" phase seen in experiments and simulations of granular materials at low volume fraction (Aharonov and Sparks, 2002, and references therein). In the simulations, the power spectrum (the absolute square of the Fourier transform) $P(\omega)$ of the shear stress on the wall was found to be white noise in the fluid phase. The analogous quantity in our model is the power spectrum of the time series of stress on the moving boundary. The model also yields white noise $P(\omega) \sim \omega^0$ for $v << v^*(\varepsilon)$, further confirming the agreement between the simulations and our MFT results. The MFT predicts universal scaling exponents and scaling functions near the critical point $\varepsilon = 0$ and $cv = 1$, as in the earlier versions of the model (Fisher *et al.*, 1997; Dahmen *et al.*, 1998). The source time functions of the avalanches near the critical point are predicted to have as before, on the average, parabolic and exponential shapes for event sizes measured by duration and moment, respectively (Mehta *et al.*, 2006).

3.4. A Unifying Phase Diagram for Shear Deformation

We now attempt to provide a general treatment for material deformation under shear. The goal is to have a framework that may be tuned to describe different dynamic regimes and different types of deforming materials, from granular media to damaged brittle and plastic or hardening solids, and possibly even to porous solids. One basic difference between solids and granular materials is the presence of cohesion C: solids have cohesion ($C > 0$) that provides strength (nonzero elastic modulus and frictional resistance) under tension. Granular materials have no cohesion to first order ($C = 0$) and hence no strength under tension. It is also important to make a distinction between cracks and voids. The former are internal surfaces with reduced cohesion, which produce stress concentrations, and hence tend to promote further failures at the crack tip. In contrast, voids are internal volumes that are devoid of material, and hence tend to diffuse stress concentrations and suppress the continuation of failures.

Crack generation in solids is associated with a cohesion drop $\Delta C = (C_i^{\text{initial}} - C_i^{\text{final}})/(\tau_{s,i} - \tau_{a,i}) > 0$, while crack healing leads to cohesion regaining. Slip avalanches in granular materials usually have no cohesion change $\Delta C = 0$. Dislocation events in plastic deformation also have no cohesion change since they do not increase the internal surface area. Porous solids under shear can form compaction bands with associated hardening (Wong *et al.*, 2001; Baud *et al.*, 2004). Though different in nature, this hardening is expected to have somewhat similar

effects on the avalanche dynamics as an increase in cohesion ($\Delta C < 0$) would have. At high pressures porous solids can also respond with cataclastic flow that is similar to deformation of granular materials. While crack extension tends to produce weakening and localization, distributed damage around a growing crack (i.e., process zone) and in the bulk may allow for small amounts of slip along the cracked surfaces. As a result, similar to voids, distributed damage leads to some relaxation of the stress accumulation while a crack is growing.

Crack healing can occur on short timescales of minutes to hours through inelastic yielding at geometrical asperities across surface areas that are in contact (Dieterich and Kilgore, 1996; Johnson and Jia, 2005; Wu *et al*., 2009; Ben-David *et al*., 2010). On the other hand, the healing of voids requires mineral deposition and is associated with longer timescales (e.g., Hickman and Evans, 1992; Chester *et al*., 1993; Bruhn *et al*., 1994). This allows for separation of timescales in the dynamics associated with evolution of cracks and voids. In the model discussed below we assume the grain volume fraction v remains unchanged over short to moderate timescales, whereas the cohesion C over contact areas can evolve. Combining these considerations with previous model results (Fisher *et al*., 1997; Dahmen *et al*., 1998, 2009, 2011; Ben-Zion *et al*., 1999, 2003; Mehta *et al*., 2006) we propose a dynamic phase diagram for sheared solids, granular materials, and porous solids with three basic ingredients that serve as tuning parameters: (1) the strength-change parameter ε, (2) an effective void fraction $(1 - cv)$ that controls the effective porosity or distributed damage and the related degree of dissipation of elastic stress transfer during spontaneous failures, and (3) the ratio Q (=shear-rate/healing-rate) that governs the effective healing of cohesion drops ΔC during brittle failures in solids under ongoing loading. Below we describe the algorithm for the extended version of the model that has the added concepts of a long-term cohesion drop ΔC with slow material re-healing and the parameter Q, starting for completeness with the simpler early version. We then present a summary of analytical model results obtained with MFT for different dynamic regimes and different types of materials.

3.4.1 *Basic Model Algorithm with Short Term Weakening Described by the Tuning Parameter ε (but in the Absence of Voids ($v = 1$) and Cohesion Drops ($\Delta C = 0$ and $Q = 0$))*

Initially the system is in a stable state with random local stresses τ_i. The algorithm for the slip avalanches in mean field theory is as follows:

1. Each site i remains stable (stuck) as long as $\tau_i < \tau_{f,i}$, where $\tau_{f,i}$ is a random local failure stress that can be static or dynamic: $\tau_{f,i} \equiv \tau_{s,i}$ or $\tau_{d,i}$. The threshold for failing first time in an avalanche is $\tau_{s,i}$. This initial static failure stress $\tau_{s,i}$ is quenched and randomly distributed in the lattice according to narrow parabolic distribution. As mentioned, the exact shape of the distribution does not affect the scaling behavior.

2. The stress at each site is slowly increased (by the moving boundary or increased stress there), until one occupied site i reaches its failure stress $\tau = \tau_{f,i}$. This starts the clock to measure the avalanche duration. One failure event takes a time $\Delta t = 1$.

3. The failing site i slips by an amount $\Delta u_i = (\tau_{f,i} - \tau_{a,i})/(J + K_L)$, i.e., it slips until τ_i is reduced to its random arrest stress $\tau_{a,i}$ and it then resticks.

4. The failure threshold of the slipped site is reduced from its static value $\tau_{f,i} = \tau_{s,i}$ to a dynamic value $\tau_{f,i} = \tau_{s,i} - \varepsilon(\tau_{s,i} - \tau_{a,i})$ where ε is the strength change parameter.

5. The stress drop $\Delta\tau_i \equiv (\tau_{f,i} - \tau_{a,i})$ leads to a stress increase at all the other sites $j \neq i$ by an amount $\Delta\tau_j = J/N(\tau_{f,i} - \tau_{a,i})/(J + K_L)$. The total redistributed stress is then $\sum_{j=1}^{N} \Delta\tau_j = (\tau_{f,i} - \tau_{a,i})J/(J + K_L) = c(\tau_{f,i} - \tau_{a,i})$ with $c \equiv J/(J + K_L)$. For large systems $K_L \sim 1/L << J$, $c \approx 1$ so the redistributed stress is approximately equal to the original stress drop $(\tau_{f,i} - \tau_{a,i})$.

6. During the next time step of duration $\Delta t = 1$, all occupied sites j with new stresses $\tau_j + \Delta\tau_j > \tau_{f,j}$ are slipped simultaneously and their stress drops are redistributed to the other sites following the rules in steps (3)–(5). The momentary slip rate of the system is the sum of all simultaneously occurring slip displacements Δu_j divided by the duration of the slip event $\Delta t = 1$. This slip rate is

also called the potency (or moment) rate at that time interval.

7. Step (6) is repeated until there are no more occupied sites exceeding their failure stresses, i.e., the avalanche has ended.

8. The failure stresses of all sites i are reset back to their static values: $\tau_{f,i} = \tau_{s,i}$. The total duration T of the avalanche is the sum of all time steps $\Delta t = 1$ for all failure episodes during the avalanche. The avalanche duration clock is reset to zero. The total size S or the potency of the slip avalanche per unit failure area is defined to be the sum of all slip displacements Δu_i that took place during the avalanche.

9. The algorithm returns to (1) with a slow increase in stress due to the boundary conditions until a new avalanche is triggered.

3.4.2 *Algorithm in the Presence of Voids and the Effective Porosity (1−cv)*

As discussed above, both solids and granular materials can have variable amounts of voids and/or distributed cracks associated with "porosity" or "damage". This is accounted for by the parameter $(1-cv)$ where v is the volume fraction occupied by undamaged material and the geometrical factor $c \approx 1$ for large systems. In our model v corresponds to the number fraction of occupied sites in the lattice (Dahmen *et al*., 2011).

3.4.3 *Extension of the Algorithm to Include Cohesion Drops ΔC and the Persistence Parameter Q*

In order to account for long term cohesion changes in solids under brittle deformation, we assume that during brittle failure the local threshold changes to a dynamic threshold $\tau_{d,i} = \tau_{s,i} - (\varepsilon + \Delta C)\ (\tau_{s,i} - \tau_{a,i})$. Here $\Delta C\ (\tau_{s,i} - \tau_{a,i})$ quantifies the dynamic cohesion drop in the case of brittle solids, while $\varepsilon(\tau_{s,i} - \tau_{a,i})$ describes the shorter term strength change (e.g., frictional weakening) of the original algorithm. This means that at the end of each avalanche the dynamic strength changes due to the term $\varepsilon(\tau_{s,i} - \tau_{a,i})$ reheal to their static values as before. However, it takes longer to reheal a cohesion drop $\Delta C(t)$, so between avalanches the new failure threshold (for brittle solids) is now given by $\tau_{f,i} = \tau_{s,i} - \Delta C(t)(\tau_{s,i} - \tau_{a,i})$ with slowly healing (decreasing) $|\Delta C(t)(\tau_{s,i} - \tau_{a,i})|$. Laboratory experiments and field studies show logarithmic rehealing with time to the original threshold strength for wide ranges of materials and conditions (e.g., Dieterich and Kilgore, 1996; Marone, 1998; Johnson and Jia, 2005; Peng and Ben-Zion, 2006; Wu *et al*., 2009).

The logarithmic rehealing of the cohesion introduces a new time scale into the model that sets a physical scale for the external shear rate. Large Q (shear-rate/cohesion-healing-rate) means that the cohesion reduction ΔC persists much longer than the duration of an avalanche and the time between avalanches, so the system obtains a long term memory of prior slips. This typically leads to localization effects (e.g., Ben-Zion *et al*., 1999; Lyakhovsky and Ben-Zion, 2009). On the other hand, small values of Q mean that the cohesion drop reheals quickly and there is no effective long term memory of earlier slips. If the cohesion drop ΔC completely reheals between avalanches (i.e., $Q = 0$), then its effect on the avalanche statistics can be absorbed into the parameter ε. This is the case both for cohesionless granular materials and for dislocation slips in solids, since in both cases no long-term cohesion drop is involved.

3.4.4 *Results from Mean Field Theory*

Figure 5 and Table 1 summarize the results obtained for the generalized model with MFT. The $Q = 0$ plane of Fig. 5 corresponds to granular materials ($C = 0$) and plastic deformation. The region $Q > 0$ ($\Delta C > 0$) and $\varepsilon > 0$ corresponds to cracking brittle solids. The pink section corresponds to hardening solids. Finally, $Q < 0$ ($\Delta C < 0$) may correspond to highly porous solids where brittle instabilities lead to rapid strengthening (creation of compaction bands) that may be followed by slow progressive weakening. As before, we assume the system is large so that the geometrical factor $c \approx 1$. Detailed derivations for the cases with $\Delta C = 0$ can be found in Fisher *et al*. (1997), Dahmen *et al*. (1998, 2009, 2011) and Mehta *et al*. (2006). As described next, the generalized model provides quantitative results for a broad range of phenomena including different types of event statistics, predictions for scaling of source time functions, localized and distributed structures, and a change of

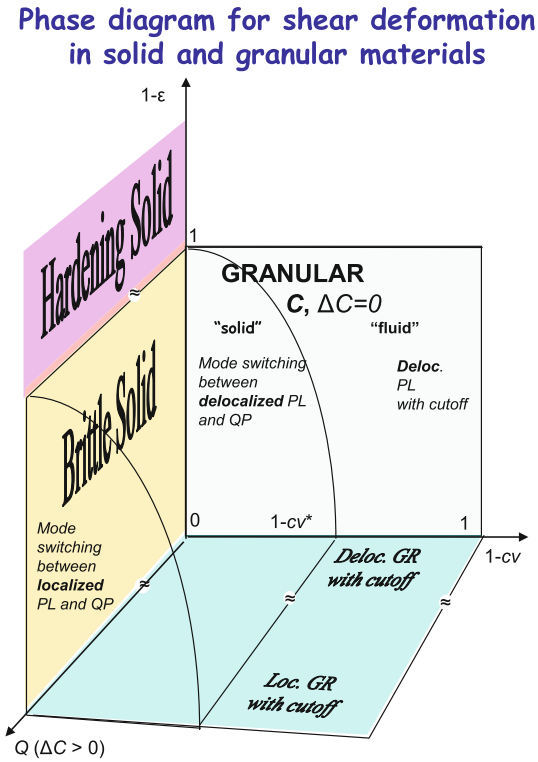

Figure 5
Phase diagram with different dynamic regimes and different material types as a function of three key tuning parameters. The diagram includes transitions from solids to granular materials ($Q = 0$, C, $\Delta C = 0$), from solid-like to fluid-like granular behavior (volume fraction $\nu \to 0$), from crystalline solid to porous solid (increasing the effective porosity $(1 - cv)$ for $Q > 0$) and from delocalized to localized deformation (increasing the effective "longevity" or persistence Q of the cohesion drop $\Delta C > 0$ from 0 to ∞). The values $\varepsilon = 0$, $1 - cv = 0$, $Q = 0$ correspond to a critical point. Hardening solids ($\varepsilon < 0$) show delocalized deformation even for effective porosity $1 - cv > 0$ with power law (PL) event statistics having ε-dependent cutoff. Porous materials are expected to be associated with $Q < 0$ (corresponding to a hardening $\Delta C < 0$)

behavior from undamaged elastic medium to damaged solid and granular material as the microscopic tuning parameters are changed. The entries in Table 1 show that the analytical model predictions are consistent overall with available laboratory and field observations and results of numerical simulations. A more detailed description of the results for different sections of the phase diagram is as follows:

$Q = 0$ ($\Delta C = 0$) and Constant Strength $\varepsilon = 0$: In the limits $\varepsilon = 0$ and $cv = 1$, mean field theory predicts power law avalanche size distributions. This point describes plastic deformation as well as granular deformation in the very dense limit. As shown in Fisher *et al.* (1997) and later related works, near this point the distribution of avalanche sizes S has the scaling form $D(S, \nu, \varepsilon) \sim 1/s^{\tau} D_w(S(1 - cv)^{1/\sigma'}, S\varepsilon^{1/\sigma''})$, where $S = \sum_i \Delta u_i$ is the total slip during the avalanche. The numerical values of the universal scaling exponents (τ, σ', σ'', α, υ', υ'', z) for this and the following scaling forms are all given in the first column of Table 1 and its caption. The distribution of the durations T of the avalanches scales as $D(T, \nu, \varepsilon) \sim 1/T^{\alpha} D_1(T(1 - cv)^{\nu' z}, T\varepsilon^{\nu'' z})$ and the power spectrum of the time trace of slip rates during avalanches is $P(\omega, \varepsilon, \nu) \sim \omega^{-1/\sigma\nu z} P_h(\omega/\varepsilon^{\nu'' z}, (1 - cv)/\varepsilon^{\sigma/\sigma'})$, where D_w, D_1, and P_h are universal scaling functions (Dahmen *et al.*, 2009, 2011). There are additional scaling functions that can be extracted from slip rate data. As mentioned in Sect. 3.2, the MFT source time function averaged over all avalanches with the same duration is a parabola, while the source time function averaged over all avalanches with the same potency/moment follows an exponential form (Mehta *et al.*, 2006; Papanikolaou *et al.*, 2009).

$Q = 0$ and Weakening $\varepsilon > 0$: For the case $cv = 1$ and $\varepsilon > 0$ it has been shown that mean field theory predicts quasi-periodically recurring abrupt large failure events with smaller (spatially distributed) events in between following overall the characteristic distribution (e.g., Fisher *et al.*, 1997; Dahmen *et al.*, 1998). This is confirmed by numerical simulations with 3D elastic stress transfer (Ben-Zion and Rice, 1993; Ben-Zion 1996; Ben-Zion *et al.*, 2003). For $\varepsilon > 0$ and $cv^* < cv < 1$, mean field theory predicts mode switching between power law and characteristic behavior, and for $\nu < \nu^*$ mostly small avalanches occur (Dahmen *et al.*, 2011) in a fluid like behavior of the granular medium for $Q = 0$, where $cv^* \equiv 1/(1 + \varepsilon)$. Similar mode switching behavior has been seen in simulations and experiments with granular media in the solid regime (Aharonov and Sparks., 2004; Hayman *et al.*, 2011), in simulations with a continuum damage rheology model (Ben-Zion *et al.*, 1999; Lyakhovsky *et al.*, 2001), and possibly in long records of localized earthquake fault zones (Marco *et al.*, 1996; Amit *et al.*, 2002).

$Q = 0$ and Strengthening $\varepsilon < 0$: For dislocation slip avalanches in solids (i.e., $\nu = 1$ and

$Q = \Delta C = 0$), in some cases there is threshold strengthening ($\varepsilon < 0$) in hardening materials due to energy absorption via processes like dislocation entanglement (Mehta *et al.*, 2006). To model this situation in MFT, when a site fails the failure thresholds of all other sites are strengthened by an amount that is proportional to ε/N. It has been shown that for solids the amplitude of $\varepsilon < 0$ is proportional to the hardening coefficient of hardening plastic materials (Dahmen *et al.*, 2009). After a failure avalanche is finished the thresholds may slowly reheal (weaken) back to their original strengths. For slow enough rehealing the model leads to aftershocks as also seen in earthquake data and experiments. The scaling forms above apply in this case to the aftershocks as well. The Omori aftershock law, $dn/dt \sim 1/t^p$, for temporal evolution of the number n of events, emerges with $p = 1$ (Table 1) if the rehealing is logarithmic in time (Mehta *et al.*, 2006). In hardening materials the deformation is distributed over the entire sample (Dahmen *et al.*, 2009). For $Q = 0$ all avalanche events are expected to nucleate at random positions in the bulk, i.e., the deformation due to slip is not localized along given fault zones.

$Q \to \infty$ (with $\Delta C > 0$): In such cases the slip events are expected to take place on localized weakened fault zones. This is because for infinitely slow healing ($Q \to \infty$) the weakened cells have a permanently lowered failure threshold, and the same mean field analysis as in Dahmen *et al.* (2009) indicates that as the system is reloaded failures tend to occur again in the same "fault zone". In this case the MFT will simplify to the description of the events on the weakened fault plane, as in Fisher *et al.* (1997) and Dahmen *et al.* (1998). Since the MFT has no concept of spatial location, it renders the same scaling results for event statistics on a single fault of slips distributed throughout the bulk of a 3D material. This is the reason that in Fig. 5 the phase diagrams in the two planes for $Q = 0$ and for $Q \to \infty$ look essentially the same, except that $Q = 0$ refers to the case with distributed deformation while $Q \to \infty$ describes the case where the slips are localized to a narrow fault zone. The two "end member" cases $Q = 0$ and $Q \to \infty$ can thus be treated analytically with the same mean field analyses discussed above. The situation gets more complicated in the crossover regime $0 < Q < \infty$. Since the MFT has no concept of space, it cannot be used in the same form to describe a slip-localization transition as a function of Q. New analytical approaches and/or simulations will be needed to clarify the details of this crossover regime. However, based on our results and those of other frameworks we can map certain expectations for this regime as done next.

Expectations for the Crossover Regime $0 < Q < \infty$: Assuming that there is not too much disorder in the system, one expects for large Q that once a system-spanning fault of weakened sites develops, almost all slip takes place in this long-term weakened zone. This process is seen in simulations with damage rheology as the development of a localized earthquake fault zone (e.g., Ben-Zion *et al.*, 1999; Lyakhovsky *et al.*, 2001; Lyakhovsky and Ben-Zion, 2009). When the stress is released due to slip on such a localized fault zone, it relaxes much of the stress in the bulk as well. As for $Q \to \infty$, in this case the original version of the BZR model developed for a single fault zone can be used to describe slip evolution on the weakened fault zone with approximately undamaged solids on both sides. Therefore, in this case the same scaling behavior is expected as in the $Q \to \infty$ case. For example, as indicated in Fig. 5, for large values of Q the same event statistics is expected (with mode switching in a certain parameters range) as was originally derived for a localized fault zone (Fisher *et al.*, 1997; Dahmen *et al.*, 1998). The region of intermediate values of Q is expected to contain a disorder-dependent "localization" transition for the damage that should be analyzed in future studies. As mentioned, simulations of coupled evolution of earthquakes and faults in a regional crustal model governed by damage rheology indicate that for a certain range of Q values there will also be mode switching between quasi-periodic statistics for events localized on a weak fault zone and power law statistics of delocalized events in the bulk (Ben-Zion *et al.*, 1999; Lyakhovsky *et al.*, 2001).

4. Discussion and Conclusions

Understanding the dynamics of material deformation under shear has important implications for many

natural and man-made systems. In experiments, field observations and simulations, slowly sheared materials have been seen to respond with jerky slip events over broad ranges of scales. This holds for dislocation slip avalanches in crystals (e.g., Zaiser, 2006), granular materials (e.g., Jaeger *et al*., 1996) and earthquakes in the Earth's crust (e.g., Turcotte, 1997). As discussed in previous sections, under certain conditions the distributions $D(S)$ of total slip-event sizes S, $D(T)$ of event duration T, and the power spectrum $P(\omega)$ of the slip rate at frequency ω, are all described by power laws over two to several decades with universal exponents (τ, α, and $1/\sigma\upsilon z$) that are shared by an entire class of different materials independent of their microscopic details. Also, both earthquake and dislocation slip events often have aftershocks (i.e., small slip events triggered shortly after larger "mainshocks") following the Omori law with decay exponent $p \sim 1$ for earthquakes (e.g., Utsu *et al*., 1995). It is important to emphasize, however, that power law (PL) behavior is only seen under certain conditions. For example, relatively straight sections of earthquake faults and some granular materials can also display quasi-periodically (QP) recurring large events with only small slips in between following together the characteristic earthquake/event (CE) distribution, or mode switching between time intervals with PL distributed slip sizes and intervals with CE statistics, and not all earthquakes have aftershock sequences (e.g., Stirling *et al*., 1996; Jaeger *et al*., 1996; Daniels and Hayman, 2008; Sections. 2 and 4.3 of Ben-Zion, 2008, and references therein).

Many separate approaches have been employed to study the avalanche-like response of solids and granular materials under different conditions (see introduction). However, a model that can be used to analyze, within one framework, different dynamic regimes of plastic and brittle deformation of solids and behavior of granular media is lacking. In this work we have used key governing variables (ε, ν, Q) to generalize previous results obtained with three variants of the BZR model for dynamic of seismicity, dislocation avalanches, and granular avalanches. The results enable us to construct a unifying dynamic phase diagram (Fig. 5) for the response of solids and granular materials under shear loadings. Increasing the effective porosity $(1 - c\nu)$ in granular materials corresponds to tuning the behavior from solid like to fluid like. Increasing the value of $(1 - c\nu)$ in solids tunes the system from a dense crystalline solid to a damaged solid. Tuning the cohesion and cohesion change correspond to transitions between solids and granular media. The parameter Q (shear-rate/cohesion-healing-rate) > 0 describes the longevity or persistence of the cohesion drop ΔC between brittle failures in solids. Changing this parameter modifies the response from delocalized deformation as seen in granular materials or ductile solids (for $\Delta C = 0$, $Q = 0$), to localized deformation (for $\Delta C > 0$, $Q \gg 1$) as seen in brittle solids that develop weakened fault zones. Both Q and ν are parameters that reflect properties of the microstructure. The third tuning parameter, the dynamic strength-change ε, is an effective parameter that is expected to depend on the microstructure (ν and Q) and other properties such as the presence of lubricants.

Table 1 summarizes the types of behavior and scaling exponents for statistics of slip avalanches for (1) our MFT model predictions, (2) experimental and simulation results on deformation of granular material, (3) experiments, simulations and observations in solids sustaining plastic deformation (with dislocation slip avalanches), (4) seismicity in the Earth's crust, and (5) damage model for brittle deformation. The table shows that all five classes exhibit the same variety of dynamic regimes and, more importantly, the available scaling exponents from all classes are consistent within error-bars. The agreement between the critical exponents predicted by our model and those of experiments and observations suggest that the MFT approximation captures the fundamental aspects of the underlying physics. The results imply that the proposed unified framework can be used to study self-consistently a wide range of phenomena in solids sustaining irreversible brittle and plastic deformation and in sheared granular materials.

The unified framework may be used to analyze, with additional model developments, the evolutionary processes that lead to solid-granular transitions in the final stages of the approach to brittle instabilities, and to slower transitions of states in the intervals between large events and in the long-term dynamics of systems under shear deformation. Such results may include new predictive signals on the evolution of

various fields (e.g., stress, strain, material properties) and observables (e.g., acoustic emission and microseismicity) in space, time and size, which may help forecasting approaching instabilities and other dynamical transitions. The discussed model predictions have been tested so far only in a limited way. The entries in Table 1 with question marks indicate quantities for which (as far as we know) there is lack of observational testing. Systematic high resolution observational tests with laboratory and field data, reflecting different values of ε, ν and Q, will provide fundamental information on the validity of the proposed unifying model. The nature of the transitions between the various types of materials and crossovers between different dynamic regimes are subjects of continuing theoretical work.

Acknowledgments

YBZ acknowledges support from the National Science Foundation (grant EAR-0908903) and the US-Israel Binational Science Foundation (grant number 2008248). KD acknowledges support from NSF DMR 03-25939 (MCC) and thanks the USC Dept. of Earth Sciences and the Kavli Institute of Theoretical Physics at UC Santa Barbara for kind hospitality and support. The manuscript benefited from useful comments by Jay Finberg, Bob Behringer, and Charlie Sammis.

References

Aharonov, E., and D. Sparks (1999), *Rigidity phase transition in granular packings*, Phys. Rev E, *60*, 6890-6896.

Aharonov, E., and D. Sparks (2002), "*Shear profiles and localization in simulations of granular materials*", Phys. Rev. E *65*, 051302/1-12.

Aharonov, E., and D. Sparks (2004), *Stick-slip motion in simulated granular layers*, J. Geophys. Res, *109*, B09306.

Alava, M. J., P. K. V. V. Nukala, and S. Zapperi (2006), *Statistical models of fracture*, Advances in Physics, *55*, 349–476.

Amit, R., E. Zilberman, N. Porat, and Y. Enzel (2002), *Paleoseismic evidence for time-dependency of seismic response on a fault system - the southern Arava Valley*, Red Sea Rift, Israel, Geol. Soc. Am. Bull., *114*, 192–206.

Ashby, M. F., and C. G. Sammis (1990), *The damage mechanics of brittle solids in compression*, Pure Appl. Geophys., *133* (3), 489–521.

Baldassari A., *et al*. (2006), *Brownian forces in sheared granular matter*, Phys. Rev. Lett. *96*, 118002.

Baud, P., E. Klein, and T.-F. Wong (2004), *Compaction localization in porous sandstones: spatial evolution of damage and acoustic emission activity* J. Struct. Geol., *26*, 603-624.

Ben-David, O., S. M. Rubinstein and J. Fineberg (2010), *Slip-stick and the evolution of frictional strength*, Nature, *463*, 76-79.

Ben-Zion, Y., and J. R. Rice (1993), *Earthquake failure sequences along a cellular fault zone in a three-dimensional elastic solid containing asperity and nonasperity regions*, J. Geophys. Res., *98*, 14109-14131.

Ben-Zion, Y. (1996), *Stress, slip and earthquakes in models of complex single-fault systems incorporating brittle and creep deformations*, J. Geophys. Res., *101*, 5677-5706.

Ben-Zion, Y., K. Dahmen, V. Lyakhovsky, D. Ertas, and A. Agnon (1999), *Self-Driven Mode Switching of Earthquake Activity on a Fault System*, Earth Planet. Sci. Lett., *172*/1-2, 11-21.

Ben-Zion, Y., M. Eneva, and Y. Liu (2003), *Large Earthquake Cycles and Intermittent Criticality On Heterogeneous Faults Due To Evolving Stress and Seismicity*, J. Geophys. Res., *108*, No. B6, 2307. doi:10.1029/2002JB002121.

Ben-Zion, Y., and V. Lyakhovsky (2006), *Analysis of Aftershocks in a Lithospheric Model with Seismogenic Zone Governed by Damage Rheology*, Geophys. J. Int., *165*, 197-210. doi: 10.1111/j.1365-246X.2006.02878.x.

Ben-Zion, Y. (2008), *Collective behavior of earthquakes and faults: Continuum-discrete transitions, progressive evolutionary changes and different dynamic regimes*, Rev. Geophys. *46*, RG4006. doi:10.1029/2008RG000260.

Bruhn, R. L., W. T. Parry, W. A. Yonkee, and T. Thompson (1994), *Fracturing and hydrothermal alteration in normal fault zones*, Pure Appl. Geophys., *142*, 609–645.

Bulatov, V. V., and A. S. Argon (1994), *A stochastic model for continuum elasto-plastic behavior. I. Numerical approach and strain localization*, Model. Simul. Mater. Sci. Eng. 2, 167.

Chen, K., P. Bak, and S. P. Obukhov (1991), "*Self Organized Criticality in a crack-propagation model of earthquakes*", Phys. Rev. A *43*, 625-630.

Chester, F. M., J. P. Evans, and R. L. Biegel (1993), *Internal structure and weakening mechanisms of the San Andreas fault*, J. Geophys. Res., *98*, 771–786.

Chinnery, M. (1963), *The stress changes that accompany strike-slip faulting*, Bull. Seismol. Soc. Amer., *53*, 921-932.

Csikor, F. F., C. Motz, D. Weygand, M. Zaiser, and S. Zapperi (2007), '*Dislocation Avalanches, Strain Bursts, and the Problem of Plastic Forming at the Micrometer Scale*', Science *318*, 251-254.

Dahmen, K., D. Ertas, and Y. Ben-Zion (1998), *Gutenberg Richter and Characteristic Earthquake behavior in Simple Mean-Field Models of Heterogeneous Faults*, Phys. Rev. *E*, *58*, 1494-1501.

Dahmen, K., and Y. Ben-Zion (2009), *The physics of jerky motion in slowly driven magnetic and earthquake fault systems*, Encyclopedia of Complexity and System Science, R. Meyers (Eds.), Vol. 5, 5021-5037, Springer.

Dahmen, K. A., Y. Ben-Zion, and J. T. Uhl (2009), *A micromechanical model for deformation in disordered solids with universal predictions for stress-strain curves and related avalanches*, Phys. Rev. Lett., *102*, 175501. doi:10.1103/PhysRevLett.102.175501.

Dahmen, K. A., Y. Ben-Zion, and J. T. Uhl (2011), *A simple analytic theory for the statistics of avalanches in sheared granular materials*, Nature Physics, *7*, 554–557. doi:10.1038/NPHYS1957.

Daniels, K. E., and N. W. Hayman (2008), "*Force chains in seismogenic faults visualized with photoelastic granular shear experiments*" Journal of Geophysical Research, *113* B11411 and references therein.

Dieterich, J. H., and B. D. Kilgore (1996), *Imaging surface contacts; power law contact distributions and contact stresses in quarts, calcite, glass, and acrylic plastic*. Tectonophysics, *256*, 219-239.

Dimiduk, D. M., C. Woodward, R. LeSar, and M. D. Uchic (2006), "*Scale-Free Intermittent Flow in Crystal Plastity*", Science *312*, 1188-1190.

Falk, M. L., and J. S. Langer (1998), Dynamics of viscoplastic deformation in amorphous solids, Phys. Rev. E, 57(6), 7192–7205.

Fisher, D. S., K. Dahmen, S. Ramanathan, and Y. Ben-Zion (1997), *Statistics of Earthquakes in Simple Models of Heterogeneous Faults*, Phys. Rev. Lett., *78*, 4885-4888.

Fisher, D. S. (1998), *Collective transport in random media: from superconductors to earthquakes,* Phys. Reports*, 301*, 113-150.

Hartley, R. R. (2004), *Evolving force networks in deforming granular materials*, PhD thesis, Duke University.

Hayman, N.W., L. Ducloue, K.L. Foco, K.E. Daniels (2011), *Granular controls on periodicity of stick-slip events: kinematics and force-chains in an experimental fault*, Pure and Applied Physics, in press.

Hickman, S. H., and B. Evans (1992), *Growth of grain contacts in halite by solution transfer; Implications for diagenesis, lithification, and strength recovery, in* Fault Mechanics and Transport Properties of Rocks, edited by B. Evans and T.-F. Wong, pp. 253–280, Academic, San Diego, Calif.

Jaeger, M., S. R. Nagel, and R. P. Behringer (1996), *Granular solids, liquids, and gases*, Rev. Mod. Phys., *68*, 1259-1273.

Johnson, P. A., and X. Jia (2005), *Nonlinear dynamics, granular media and dynamic earthquake triggering*, Nature, *473*, 871-874.

Kachanov, L. M. (1986), *Introduction to continuum damage mechanics*, pp. 135, Martinus Nijhoff Publishers.

Kuntz, M. and J.P.Sethna (2000), *Noise in disordered systems: the power spectrum and dynamic exponents in avalanche models*, Phys. Rev. B *62*, 11699-11708.

Laurson, L., and M. J. Alava (2006), 1*/f noise and avalanche scaling in plastic deformation*, Phys. Rev. E *74*, 066106.

Liu, A. J., and S. R. Nagel (eds) (2001), *Jamming and Rheology*, Taylor and Francis, New York.

Lyakhovsky, V., Y. Ben-Zion, and A. Agnon (2001), *Earthquake Cycle, Fault Zones, and Seismicity Patterns in a Rheologically Layered Lithosphere*, J. Geophys. Res., *106*, 4103-4120.

Lyakhovsky, V. and Y. Ben-Zion (2008), *Scaling relations of earthquakes and aseismic deformation in a damage rheology model*, Geophys. J. Int., *172*, 651-662. doi:10.1111/j.1365-246X.2007.03652.x.

Lyakhovsky, V. and Y. Ben-Zion (2009), *Evolving geometrical and material properties of fault zones in a damage rheology model*, Geochem. Geophys. Geosyst., *10*, Q11011. doi:10.1029/2009GC002543.

Maloney, C. E. and M. O. Robbins (2009), Anisotropic *Power Law Strain Correlations in Sheared Amorphous 2D Solids*, Phys. Rev. Lett. 102, 225502.

Marco, S., M. Stein, A. Agnon, and H. Ron (1996), *Long term earthquake clustering: a 50,000 year paleoseismic record in the Dead sea graben*, J. Geophys. Res.*, 101*, 6179-6192.

Marone, C. (1998), *Laboratory-derived friction laws and their application to seismic faulting*, Annu. Rev. Earth Planet. Sci.*, 26*, 643-649.

Mehta, A. P., K. A. Dahmen, and Y. Ben-Zion (2006), *Universal mean moment rate profiles of earthquake ruptures*, Phys. Rev. E., *73*, 056104.

Papanikolaou, S., F. Bohn, R. L. Sommer, G. Durin, S. Zapperi, and J. P. Sethna (2009), *Beyond scaling: the average avalanche shape*, arXiv:0911.2291.

Peng, Z., and Y. Ben-Zion (2006), *Temporal changes of shallow seismic velocity around the Karadere-Duzce branch of the north Anatolian fault and strong ground motion*, Pure Appl. Geophys., *163*, 567-600. doi:10.1007/s00024-005-0034-6.

Petri, A., A. Baldassarri, F. Dalton, G. Pontuale, L. Pietronero, S. Zapperi, (2008) *Stochastic dynamics of a sheared granular medium*, EPJ B *64*, 531.

Rechenmacher, A., Abedi, S. and Chupin, O. (2010), Evolution of Force Chains in Shear Bands in Sand, Geotechnique, *60*, 343-351.

Richeton, T., J. Weiss, and F. Louchet (2005), *Breakdown of avalanche critical behavior in polycrystalline plasticity*, Nature Materials *4*, 465-469.

Sethna, J.P., K. A. Dahmen, and C. R. Myers (2001), "*Crackling Noise*", Nature, *410*, 242-250.

Spaepen, F. (1977), *A microscopic mechanism for steady state inhomogeneous flow in metallic glasses*,*Acta Metallurgica 25*, *407*-415.

Tsekenis, G. and K. A. Dahmen (2010) *Depinning without a Jamming Point in Dislocation Systems*, Phys. Rev. Lett., submitted.

Turcotte, D. L. (1997), *Fractals and Chaos in Geology and Geophysics*, Cambridge University Press.

Utsu, T., Y. Ogata, and R. S. Matsu'ura (1995), *The centenary of the Omori Formula for a decay law of aftershock activity*, J. Phys. Earth, *43*, 1-33.

Weertman, J. (1996), *Dislocation Based Fracture Mechanics*, World Scientific.

Wong, T.-F., P. Baud and E. Klein (2001), *Localized failure modes in a compactant porous rock*. Geophys. Res. Lett. *28*, 2521-2524.

Wu, C., Z. Peng, and Y. Ben-Zion (2009), *Non-linearity and temporal changes of fault zone site response associated with strong ground motion*, Geophys. J. Int., *176*, 265–278. doi: 10.1111/j.1365-246X.2008.04005.x.

Yu, P., T. Shannon, B. Utter, R.P. Behringer (2009), *Stick-Slip in a 2D Granular Medium*", submitted.

Zaiser, M. (2006), *Scale invariance in plastic flow of crystalline solids*, Advances in Physics *55*, 185-245.

Miguel M.C. and Zapperi, S. (2006), *Fluctuations in plasticity at the microscale,* Science 312, 1151-1152 and references therein.

Zhang, J., T.S. Majumdar, A. Tordesillas, and R.P. Behringer (2010), *Statistical Properties of a 2D Granular Material Subjected to Cyclic Shear*, Granular Matter, 12, 159–172.

(Received July 8, 2010, revised December 26, 2010, accepted December 28, 2010, Published online February 22, 2011)